



# Application of the dynamic Wilhelmy plate to identification of slippage at a liquid–liquid–solid three-phase line of contact

Aniello Mennella<sup>1</sup>, Norman R. Morrow<sup>\*</sup>, Xina Xie

Department of Chemical and Petroleum Engineering/Western Research Institute, University of Wyoming, Laramie, WY 82071-3295, USA

Received 1 October 1994; accepted 20 November 1994

---

## Abstract

The dynamic Wilhelmy plate provides force–distance records that result from the plate passing through an interface at slow constant speed. The form of these force–distance records is determined by a combination of buoyancy and capillary forces. In the present work, wetting behavior of liquid–liquid–solid systems is investigated with changes in wetting properties of silica or glass substrates induced by crude oil. Two initial plate positions are analyzed. In the first, the plate is initially suspended in air above a vessel containing brine overlain by oil. The plate is then lowered through the air–oil and oil–brine interfaces. In the second, the plate is initially immersed in brine and then raised into the oil phase. In each case, the direction of plate motion is reversed during the course of measurement. Oil–brine–solid systems commonly exhibit contact angle hysteresis. Idealized force–distance records have been calculated for which receding and advancing contact angles are constant and the three-phase line of contact remains pinned during contact angle transitions that result from reversing the direction of motion of the plate. Comparison of experimental results with the idealized behavior shows that stabilized wetting conditions are not always achieved. It was often observed that slippage of the three-phase line of contact caused the distance of plate motion over which contact angle transitions occur to be much longer than that predicted by theory.

---

## 1. Introduction

The significance of reservoir wettability to many aspects of petroleum engineering is now well recognized. The behavior of crude-oil/brine/solid three-phase contact lines is of fundamental importance to the mechanism of oil recovery by waterflooding. Commonly used methods of investigating this behavior range from measurements of contact angles exhibited by reservoir fluids at representative mineral surfaces, to characterization of wetting behavior by some form of displacement test that involves core samples (e.g.,

spontaneous imbibition, capillary pressure or waterflood behavior) (Cuiec, 1991).

The Wilhelmy plate provides a direct method of measuring adhesion tension,  $\tau$  (the product of interfacial tension,  $\sigma$ , and contact angle,  $\theta$ ) acting along the perimeter of the plate (Wilhelmy, 1863; Princen, 1970; Adamson, 1990):

$$\tau = \sigma \cos \theta \quad (1)$$

When the plate, of width  $w$  and thickness  $t$ , contacts the interface, the change in force,  $F$ , acting on the plate due to adhesion tension acting along the perimeter of the plate,  $p$ , where  $p = 2(w + t)$ , is:

$$F = \sigma p \cos \theta \quad (2)$$

\* Corresponding author.

<sup>1</sup> Present address: ENIRICERCHE S.p.A., Via Maritano 26, 20097 S. Donato Milanese (MI), Italy.

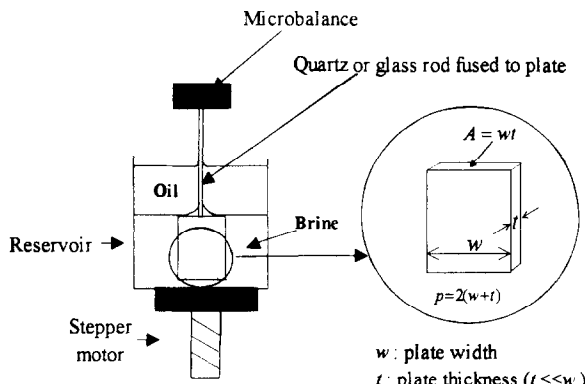


Fig. 1. The dynamic Wilhelmy plate method illustrated with the plate initially in brine.

If the interfacial tension is known, the contact angle is given by:

$$\theta = \arccos \frac{F}{\rho \sigma} \quad (3)$$

For heterogeneous wetting,  $\theta$  corresponds to an effective contact angle acting at the perimeter.

The development of the dynamic Wilhelmy plate, in which the plate is moved at constant speed through the interface between oil and brine (see Fig. 1), has been applied to the investigation of the movement of the three-phase line of contact. Crude-oil/brine/solid (COBS) systems usually exhibit contact angle hysteresis according to whether the brine/crude-oil interface is advancing or receding across the plate surface (Andersen et al., 1989; Fleureau, 1992). Advancing and receding contact angles,  $\theta_{o-w}^{adv}$  and  $\theta_{o-w}^{rec}$ , respectively, are usually measured through the aqueous phase. During transitions from, for example, advancing to receding conditions by reversal of motion of the plate, interface pinning can be expected as the contact angle

changes from  $\theta_{o-w}^{adv}$  to  $\theta_{o-w}^{rec}$ . If the force-distance record permits identification of stabilized values of  $\theta_{o-w}^{adv}$  and  $\theta_{o-w}^{rec}$ , then a complete idealized force-distance diagram can be calculated which features contact line pinning. In the present study it is shown that even if stabilized wetting is obtained, the force-distance records for wettability states induced by crude oils often show large deviation from the idealized behavior predicted for simple contact angle pinning. This deviation is referred to as anomalous pinning. In many instances, this is because the three-phase contact line slips during the contact angle transition. This behavior, referred to as slippage of the three-phase line of contact (STPL), is demonstrated by comparison of idealized results with force-distance records measured for a variety of types of wetting behavior.

## 2. Theory—Idealized force-distance relationships

The shape of the force-distance relationship recorded during a dynamic Wilhelmy plate experiment is determined by a combination of buoyancy and capillary forces. The form of these records will, therefore, be discussed in terms of idealized examples first for the plate initially in air and second for the plate initially in brine. These results will then be compared with measured data.

In discussing the form of force-distance diagrams, key points are indicated by capital letters, e.g., A, B, and the line between the points by a bar, e.g.,  $\overline{AB}$ . Surface and interfacial tensions,  $\sigma_{a-o}$  and  $\sigma_{o-w}$ , respectively, are assumed to be constant. Composition of synthetic reservoir brine and properties of the liquids used in the calculations and in the experiments are given in Table 1.

Table 1  
Physical properties of the fluids used in the present study

Fluid	Density, $\rho$ (g/cm <sup>3</sup> )	SFT, $\sigma_{a-o}$ (dynes/cm)	IFT, $\sigma_{o-w}$ (dynes/cm)
Brine <sup>a</sup>	1.0123	72	
Crude oil (Alaskan 93)	0.895	29.1	25
Decane (practical grade)	0.7211	23.8	33.5
Decane (cleaned <sup>b</sup> )	0.7211	23.6	51.5

<sup>a</sup>Synthetic reservoir brine. Composition (wt%): NaCl, 2.13; CaCl<sub>2</sub>·6H<sub>2</sub>O, 0.06; KCl, 0.01; MgCl<sub>2</sub>·6H<sub>2</sub>O, 0.02.

<sup>b</sup>Major contaminants were removed from decane by flow through silica and alumina packed columns.

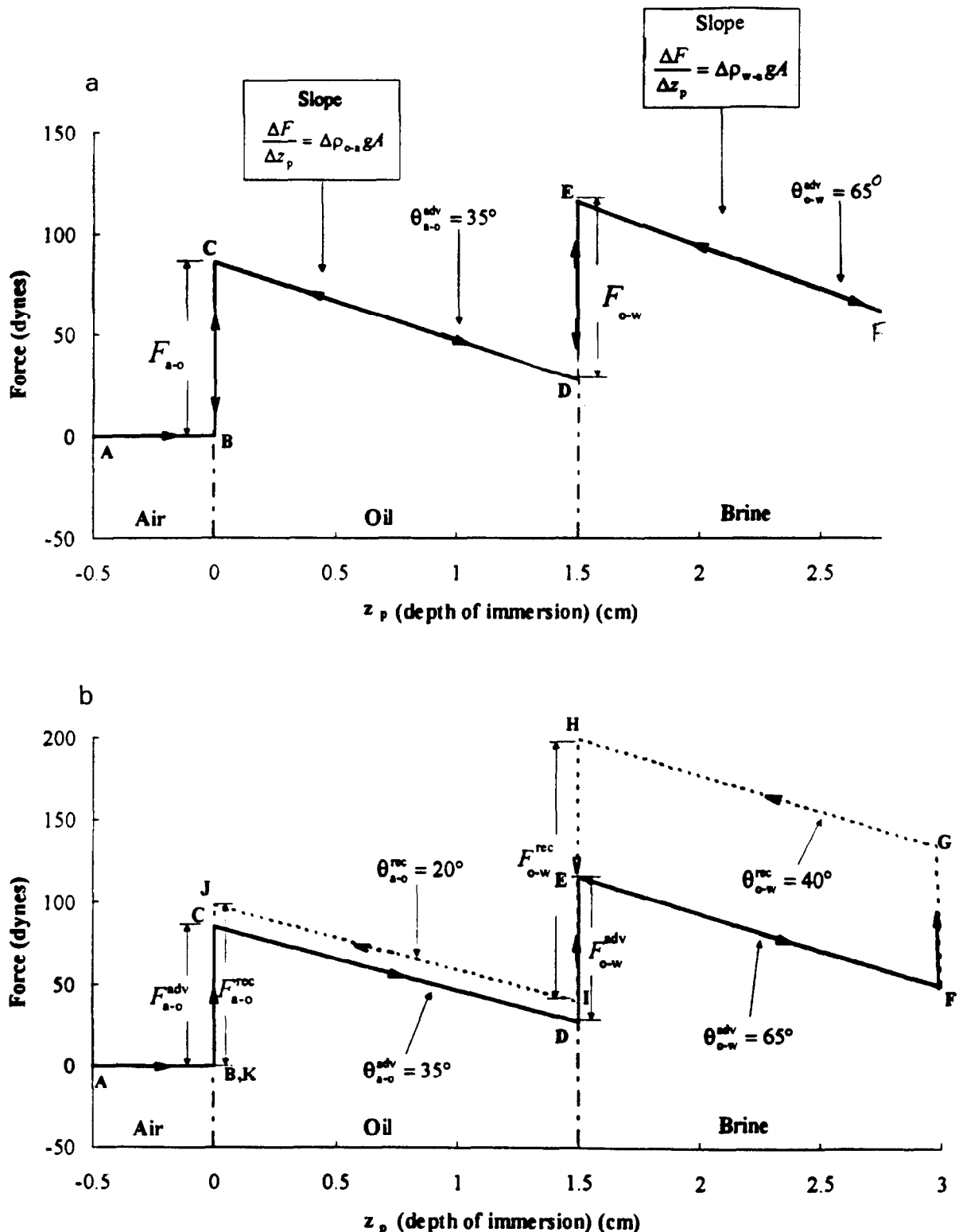


Fig. 2. Calculated force versus distance diagram. Plate initially in air (upper portion of the plate always in air). (a) No hysteresis and no pinning; (b) hysteresis and no pinning.

## 2.1. Plate initially in air

### No contact angle hysteresis

In Fig. 2a, a calculated idealized force diagram is shown for an experiment involving a gas/oil/brine/solid system with no hysteresis in both the air–oil contact angle,  $\theta_{a-o}$ , and the oil–water contact angle  $\theta_{o-w}$ .

$A \rightarrow B$ : While the slide is hanging in air and the vessel is raised at constant speed, the force remains constant.

$B \rightarrow C$ : At  $z_p = 0$  the slide touches the air–oil ( $a-o$ ) interface. A force jump, due to the capillary force acting on the slide, is given by  $F_{a-o} = p\sigma_{a-o} \cos \theta_{a-o}$ .

$C \rightarrow D$ : As the interface is raised further, the force decreases, because of the change in buoyancy given by  $\Delta F/\Delta z_p = \Delta\rho_{o-a}gA$ , where the density difference  $\Delta\rho_{o-a}$  is given by  $\rho_{oil} - \rho_{air}$  and  $A (=wt)$  is the horizontal cross-sectional area.

$D \rightarrow E$ : At  $z_p = 1.5$  the slide touches the oil–water ( $o-w$ ) interface. If the slide is water-wet, a second force jump occurs with the increase given by  $F_{o-w} = p\sigma_{o-w} \cos \theta_{o-w}$ .

$E \rightarrow F$ : The vessel is raised further. Provided part of the upper portion of the slide remains in air, the decrease in buoyancy force with distance is given by  $\Delta F/\Delta z_p = \Delta\rho_{w-ag}A$ .

When the direction of motion is reversed, with the idealized situation of no hysteresis in contact angle, and separation of the plate from the oil–water and air–oil interfaces at  $z_p = 0$  and  $z_p = 1.5$ , respectively, the force–distance path is retraced as  $\overline{FEDCBA}$ .

### Contact angle hysteresis (no pinning)

In Fig. 2b an idealized force diagram is shown for a gas/oil/brine/solid system with hysteresis in both  $a-o$  and  $o-w$  contact angles. The receding and advancing contact angles will be denoted as  $\theta_{a-o}^{rec}$  and  $\theta_{a-o}^{adv}$ , respectively, for the air–oil interface, and  $\theta_{o-w}^{rec}$  and  $\theta_{o-w}^{adv}$ , respectively, for the oil–water interface.

When the direction of plate movement is reversed, it will be assumed that the contact angles change immediately from advancing to receding. It will also be assumed that separation of the plate from the two interfaces occurs at  $z_p = 1.5$  and  $z_p = 0$ . These assumptions are physically unrealistic because contact angle transitions and the true plate separation behavior are ignored. However, the force diagram obtained using

these assumptions defines the features that are essential to the interpretation of the measured data.

When the slide enters the oil phase and then passes through the liquid–liquid interface, the force–distance path  $\overline{ABCDEF}$  has the same form as for the idealized system with no hysteresis (see Fig. 2a) but with the force jumps being denoted by  $F_{a-o}^{adv}$  and  $F_{o-w}^{adv}$ . The return path, shown in Fig. 2b as  $\overline{FGHEIJCKA}$  consists of the following parts.

$F \rightarrow G$ : The direction of motion is reversed. A shift in the force given by  $\Delta F = (F_{a-o}^{rec} - F_{a-o}^{adv}) + (F_{o-w}^{rec} - F_{o-w}^{adv})$  is recorded. This shift is due to hysteresis in both  $\theta_{a-o}$  and  $\theta_{o-w}$ .

$G \rightarrow H$ : The recorded force now increases, because of buoyancy reduction, with the same slope  $\Delta F/\Delta z_p$  as for the change  $E \rightarrow F$  (lines  $\overline{EF}$  and  $\overline{GH}$  are parallel).

$H \rightarrow I$ : When the  $o-w$  interface detaches from the slide, the force jumps to a reduced value. The reduction in force is given by  $F_{o-w}^{rec} = p\sigma_{o-w} \cos \theta_{o-w}^{rec}$ .

$I \rightarrow J$ : As the vessel holding the two liquids is lowered further, the force increases, because of buoyancy reduction, at the same rate as in step  $C \rightarrow D$  (lines  $\overline{IJ}$  and  $\overline{CD}$  are parallel).

$J \rightarrow K$ : At point J, the slide detaches from the  $a-o$  interface and the force falls to the initial value ( $F=0$ ). The decrease is given by  $F_{a-o}^{rec} = p\sigma_{a-o} \cos \theta_{a-o}^{rec}$ .

The force jumps  $F_{a-o}^{adv}$ ,  $F_{a-o}^{rec}$ ,  $F_{o-w}^{adv}$  and  $F_{o-w}^{rec}$  divided by the geometrical perimeter  $p$  of the plate give the corresponding adhesion tensions  $\tau_{a-o}^{adv}$ ,  $\tau_{a-o}^{rec}$ ,  $\tau_{o-w}^{adv}$  and  $\tau_{o-w}^{rec}$ . If the surface tension,  $\sigma_{a-o}$ , and the interfacial tension,  $\sigma_{o-w}$ , are known, the contact angles  $\theta_{a-o}^{adv}$ ,  $\theta_{a-o}^{rec}$ ,  $\theta_{o-w}^{adv}$  and  $\theta_{o-w}^{rec}$  are given by:

$$\cos \theta_{a-o}^{adv} = \frac{F_{a-o}^{adv}}{p\sigma_{a-o}} \quad (4a)$$

$$\cos \theta_{a-o}^{rec} = \frac{F_{a-o}^{rec}}{p\sigma_{a-o}} \quad (4b)$$

$$\cos \theta_{o-w}^{adv} = \frac{F_{o-w}^{adv}}{p\sigma_{o-w}} \quad (4c)$$

$$\cos \theta_{o-w}^{rec} = \frac{F_{o-w}^{rec}}{p\sigma_{o-w}} \quad (4d)$$

### Contact angle hysteresis with pinning

For systems that exhibit contact angle hysteresis, reversal of the plate motion must involve a region of contact angle transition. During this period, the three-

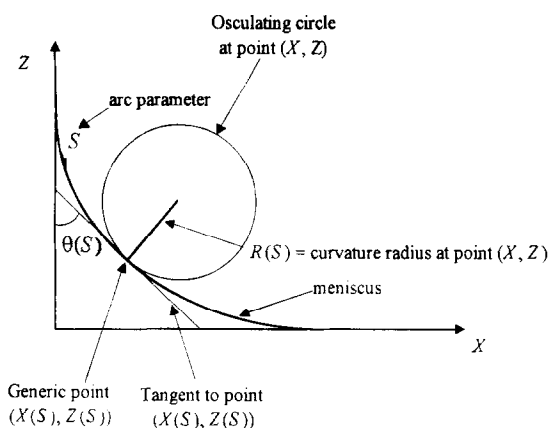


Fig. 3. Geometry of capillary rise against an infinite vertical plate. Plate position,  $X$ , is determined by the contact angle,  $\theta$ .

phase line of contact is fixed and vertical movement of the interface with respect to the plate is compensated by change in the contact angle acting at the plate. The distance over which pinning occurs depends on the values of the advancing and receding contact angles and of the capillary constant  $a_{o-w} = \sqrt{2\sigma_{o-w}/(\rho_{water} - \rho_{oil})g}$ .

The pinning distance for any pair of receding and advancing contact angles can be calculated from the solution of the Young and Laplace equation for capillary rise of a liquid against an infinite vertical flat surface.

The curvature of the meniscus at a generic point  $(X, Z)$  (see Fig. 3) can be written as:

$$\frac{1}{R} = \left[ \left( \frac{d^2X}{ds^2} \right)^2 + \left( \frac{d^2Z}{ds^2} \right)^2 \right]^{1/2} = \frac{d\theta}{ds} \quad (5)$$

The balance between the capillary pressure  $P_c = \sigma/R$  and the gravitational head  $\Delta\rho g Z$  along with the parametric equations for  $dX(s)/ds$  and  $dZ(s)/ds$  leads to the following system of differential equations:

$$\frac{d\theta}{ds} = \frac{2}{a^2} Z \quad (6a)$$

$$\frac{dZ}{ds} = -\cos \theta \quad (6b)$$

$$\frac{dX}{ds} = \sin \theta \quad (6c)$$

where  $a^2 = 2\sigma/\Delta\rho g$  is the capillary constant. In terms of the dimensionless variables  $x = X/a$ ,  $z = Z/a$  and  $s = S/a$ , Eqs. 6a,b and c become:

$$\frac{d\theta}{ds} = 2z \quad (7a)$$

$$\frac{dz}{ds} = -\cos \theta \quad (7b)$$

$$\frac{dx}{ds} = \sin \theta \quad (7c)$$

Exact solutions in terms of  $\theta(z)$  and  $x(z)$  are given by:

$$\theta(z) = \begin{cases} \arcsin(1-z^2) \\ \pi - \arcsin(1-z^2) \end{cases} \quad (8a)$$

where  $z > 0$  corresponds to capillary rise and  $z < 0$  corresponds to capillary depression.

$$x(z) = \frac{1}{2} \left[ 2(1 - \sqrt{2-z^2}) - \sqrt{2} \ln \left( \frac{(2+\sqrt{2})z}{(2+\sqrt{2}\sqrt{2-z^2})} \right) \right] \quad (8b)$$

Budziak and Neumann (1990) used the height of the capillary rise ( $z = h$ ) to calculate contact angle from the relation:

$$\sin \theta = 1 - \left( \frac{h}{a} \right)^2 \quad (9)$$

Application of Eqs. 8a and b allows the force diagram to be calculated for a given system, if advancing and receding contact angles, densities of the fluids, surface and interfacial tensions, geometrical dimensions of the plate, thickness of the oil layer and maximum immersion depth are known. Pinning of the three-phase line of contact during contact angle transitions is included in the calculations. Interface attachment or separation sometimes involves pinning at the corners of the lower and upper edges of the plate. This effect is included in the calculated force-distance diagrams shown in Figs. 4–8.

#### Water-wet plate

Fig. 4 shows the calculated force versus distance behavior for a water-wet plate for the assumed values of advancing and receding contact angles shown in the

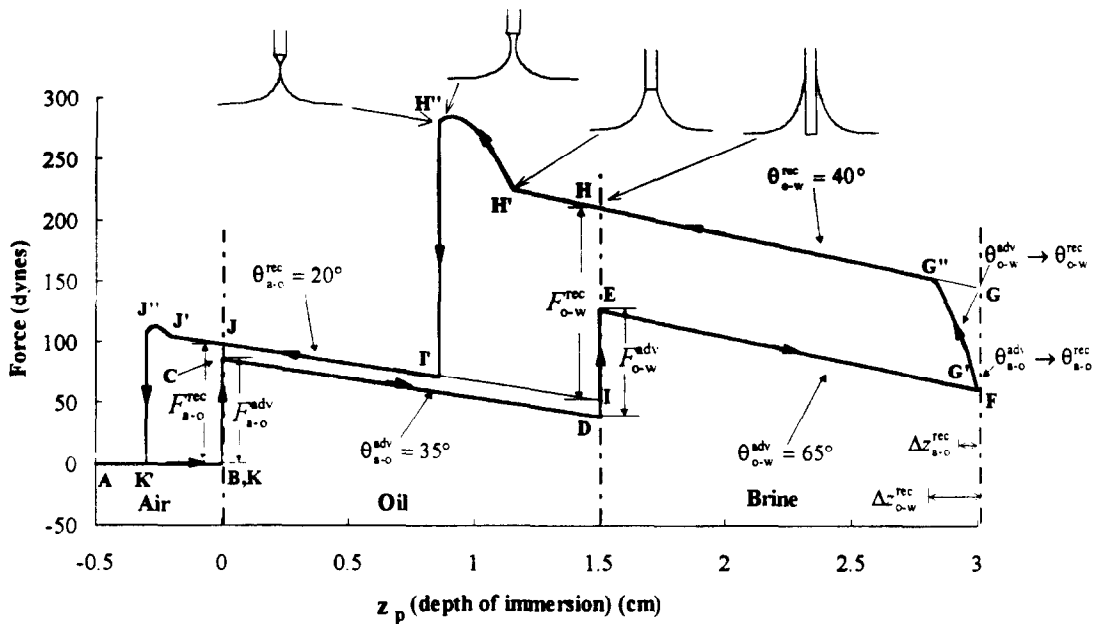


Fig. 4. Calculated force versus distance diagram with contact angle hysteresis and pinning. Plate initially in air (water wet plate).

figure. Lowering of the plate from air corresponds to the path ABCDEF. At F, the direction of motion is reversed. The effects of contact line pinning can be seen by comparing Fig. 4 and Fig. 2b.

$F \rightarrow G'$ : Both the a-o and o-w contact lines are pinned. At point  $G'$  a stable receding contact angle is established at the a-o interface but the o-w contact line is still pinned. The pinning distance of the a-o contact line (given by the projection of line  $\overline{FG'}$  onto the  $z_p$  axis) is given by  $\Delta z_{a-o}^{rec} = a_{a-o}(\sqrt{1 - \sin \theta_{a-o}^{rec}} - \sqrt{1 - \sin \theta_{a-o}^{adv}})$

$G' \rightarrow G''$ : Between points  $G'$  and  $G''$  only the o-w contact line is pinned (the total pinning distance,  $\Delta z_{o-w}^{rec} = a_{o-w}(\sqrt{1 - \sin \theta_{o-w}^{rec}} - \sqrt{1 - \sin \theta_{o-w}^{adv}})$ , usually exceeds and hence incorporates  $\Delta z_{a-o}^{rec}$ ).

$G'' \rightarrow H'$ : At point  $G''$ , a stable o-w contact angle is established and the force increases linearly because of decrease in buoyancy.

$H' \rightarrow H''$ : At point  $H'$  the o-w contact line and the bottom edge of the plate coincide. As the plate is withdrawn further the o-w interface remains attached to the plate edge (see Fig. 4) until, for a plate of infinite width, the two sides of the meniscus touch.

$H'' \rightarrow I'$ : At point  $H''$ , the interface detaches from the plate. The rupture condition (see Fig. 4) is given by  $a_{o-w}x(z) = t/2$ , where  $t$  represents the plate thickness

and  $z = z_{max}/a_{o-w}$  where  $z_{max}$  is the maximum meniscus height above the o-w interface.

$J' \rightarrow J''$ : Between points  $J'$  and  $J''$  the behavior for the air-oil interface is comparable to  $H' \rightarrow H''$  for the oil-water interface. The rupture condition is given by:  $a_{a-o}x(z) = t/2$ , where  $z = z_{max}/a_{a-o}$  and  $z_{max}$  is the maximum meniscus height above the a-o interface.

#### Hybrid-wet plate

For crude-oil/brine wetting, low receding contact angles and high advancing contact angles are sometimes observed. Assumed contact angles and characteristic results for such systems are shown in Fig. 5.

$D \rightarrow E'$ : When the plate is immersed, the force-distance diagram corresponds to that shown in Fig. 4 until point D is reached. As the plate enters the water, the three-phase line of contact remains pinned until the advancing contact angle of  $165^\circ$  is established at  $E'$ . The pinning distance is given by  $|z_{o-w}^{adv}|$  where  $z_{o-w}^{adv} = \text{sgn}(\cos \theta_{o-w}^{adv}) a_{o-w} \sqrt{1 - \sin \theta_{o-w}^{adv}}$ .

$E' \rightarrow F$ : The force acting on the plate decreases linearly.

$F \rightarrow G'$ : When the direction of plate motion is reversed, the two interfaces are pinned.  $\theta_{a-o}^{adv}$  is established at  $G'$ . The oil-water three-phase contact line

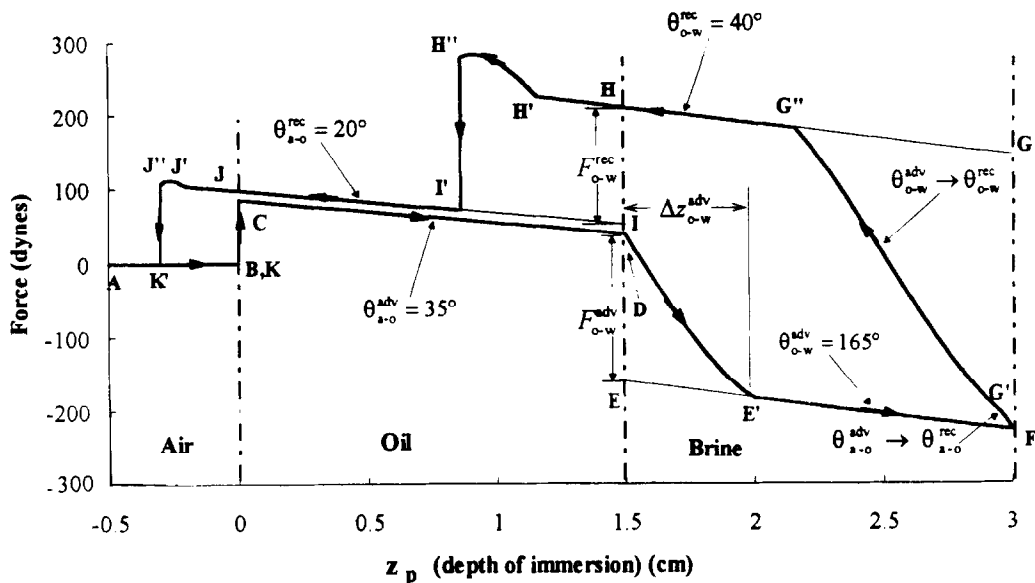


Fig. 5. Calculated force versus distance diagram with contact angle hysteresis and pinning. Plate initially in air (hybrid wet plate).

remains pinned from F to  $G''$  as the contact angle decreases from  $165^\circ$  to  $40^\circ$ .

$G' \rightarrow H'':$  Once the oil–water receding contact angle is established at  $G''$ , the behavior over the path  $G''H''H'I'J'J'K'A$  corresponds to that described for the example shown in Fig. 4a.

#### Oil-wet plate

Fig. 6 shows the calculated force diagram for an oil-wet plate ( $\theta_{o-w}^{adv} = 165^\circ$ ,  $\theta_{o-w}^{rec} = 140^\circ$ ). The characteristics of the diagram are the same as Fig. 5, for the path ABCDE'FG'.

$F \rightarrow G'':$  Because  $\theta_{o-w}^{rec}$  is high, the pinning distance after motion reversal is small, but still larger than the

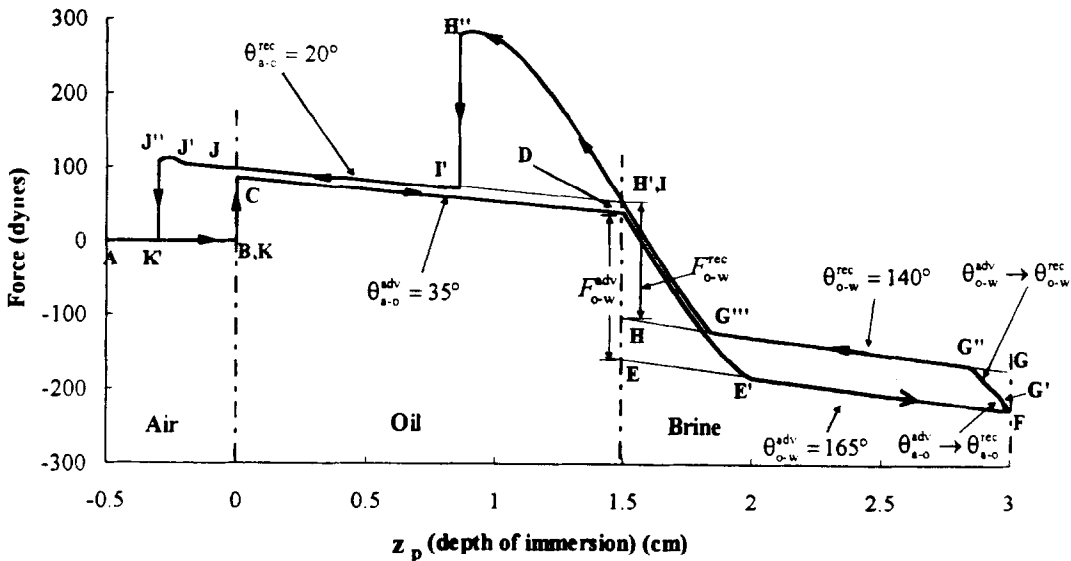


Fig. 6. Calculated force versus distance diagram with contact angle hysteresis and pinning. Plate initially in air (oil-wet plate).

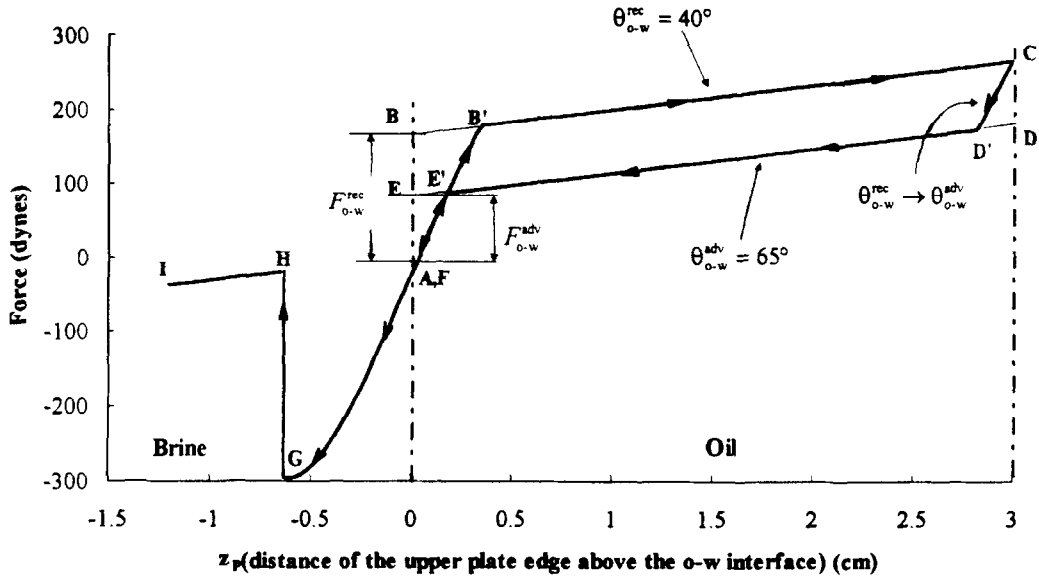


Fig. 7. Calculated force versus distance diagram. Plate initially in water (water wet plate).

a-o pinning distance given by the projection of  $\overline{FG'}$  on the depth axis.

$G'' \rightarrow G'''$ : The three-phase contact line moves with respect to the plate with  $\theta_{o-w}^{rec}$  at  $140^\circ$  and  $\theta_{a-o}^{rec}$  at  $20^\circ$ .

$G''' \rightarrow H'$ : The theoretical pinning distance due to the o-w interface hanging from the plate edge is much greater than for the wetting conditions illustrated in Fig. 4 and Fig. 5.

$H'' \rightarrow I'$ : The plate detaches from the oil–water interface and so on.

## 2.2. Plate initially in brine

### Water-wet plate

Fig. 7 shows the calculated force versus distance plot for a water-wet plate initially in brine. In experimental work, the plate is suspended from the balance by a rod which connects to the top edge of the plate. The reference level,  $z_p = 0$ , is set at point A, with the top edge of the plate at  $z_p = 0$ . The capillary forces acting on the rod at the a-o and o-w interfaces, (denoted by  $F_{a-o}^{rod}$  and  $F_{o-w}^{rod}$ , respectively) at the beginning of the experiment are tared out (Mennella and Morrow, 1995). A correction for the change in force resulting from raising the rod above the o-w interface was made assuming a rod diameter of 1 mm and that the receding contact angle acting at the rod was equal to that acting at the plate.

$A \rightarrow B'$ : As the plate is raised above the o-w level, the interface is pinned until a stable receding angle ( $\theta_{o-w}^{rec}$ ) is established at  $B'$ . The force jump,  $F_{o-w}^{rec}$ , that defines  $\theta_{o-w}^{rec}$ , is given by the length of the line  $\overline{AB}$  plus  $F_{o-w}^{rod}$ .

$B' \rightarrow C$ : A linear increase in force, because of decrease in buoyancy, is given by  $\Delta F/\Delta z_p = g[\Delta\rho_{o-a}\pi R_{rod}^2 + \Delta\rho_{w-o}A]$ , where  $R_{rod}$  is the radius of the rod.

$C \rightarrow D'$ : When the motion is reversed at C, the contact line is pinned again until the advancing contact angle ( $\theta_{o-w}^{adv}$ ) is established at  $D'$ .

$D' \rightarrow E'$ : The force decreases linearly; the path is parallel to  $\overline{B'C}$ . The force jump,  $F_{o-w}^{adv}$  is given by the length of the line  $\overline{AE}$  plus  $F_{o-w}^{rod}$ .

$E' \rightarrow G$ : At  $E'$ , the o-w interface is pinned. As the plate is dipped further into the water, it is assumed that pinning continues at the upper edge of the plate until the interface detaches at point G.

$H \rightarrow I$ : The force at H and the slope of  $\overline{HI}$  are determined by rod buoyancy.

### Hybrid-wet plate

Fig. 8 shows the calculated force diagram for a hybrid-wet plate. The path from A to C is identical to that shown for water receding conditions in Fig. 7.

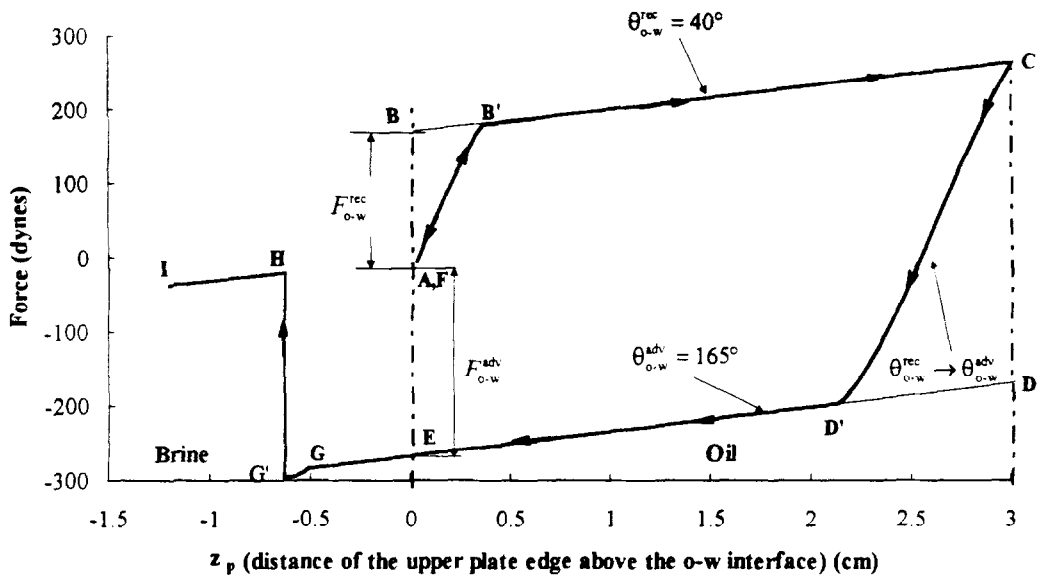


Fig. 8. Calculated force versus distance diagram. Plate initially in water (hybrid wet plate).

C → D': The interface is pinned until the advancing contact angle is established at point D'. The negative force jump  $F_{o-w}^{adv}$  is given by the length of the line EF plus  $F_{o-w}^{rod}$ .

D' → G: The force decreases linearly. At  $z_p = 0$  (point E), in contrast to the water-wet case, the interface is depressed and the force is negative.

G → G': The interface is pinned at the upper edge of the plate until detachment at point G'.

### 3. Comparison of theoretical and experimental curves

In the present work, the sole consideration in selecting the presented results was to provide examples of different types of wetting behavior. Plates were initially cleaned in a solution of 30%  $H_2O_2$  and 20%  $NH_4OH$  and washed with distilled water. The plates were then equilibrated for 10 days in a synthetic reservoir brine. Subsequent treatment of the plates and other experimental conditions corresponding to the results presented in Figs. 9–13 are summarized in Table 2.

In Figs. 9–13 interpretation of results, the interfacial tension was assumed to be at its equilibrium value (Mennella and Morrow, 1995). Comparison of experimental and theoretical curves demonstrates the advan-

tages and limitations of the standard method for calculating contact angles from force versus distance records.

In Figs. 9–13, the lettering convention for the calculated curve is maintained. Results from experiments are shown as dashed lines. Special points that relate specifically to the experimental results are indicated with lower case letters. From these figures it can be seen that force versus distance diagrams obtained by experiment can be significantly different from the theoretical results of the type shown in Figs. 4–8.

Table 2  
Summary of plate preparation and experimental conditions

Fig. No.	Plate preparation <sup>a</sup>	Oil phase in plate test	Initial plate position
9	Air dried	Crude oil	In air
10	Adsorption from crude oil <sup>b</sup>	Decane	In air
11	Adsorption from crude oil <sup>b</sup>	Crude oil	In air
12	Plate remains immersed in brine	Clean decane	In brine
13	Adsorption from crude oil <sup>b</sup>	Crude oil	In brine

<sup>a</sup>Following cleaning and equilibration in synthetic reservoir brine.

<sup>b</sup>Plate with brine film immersed in crude oil and aged for 72 hours at 88°C; then washed with toluene.

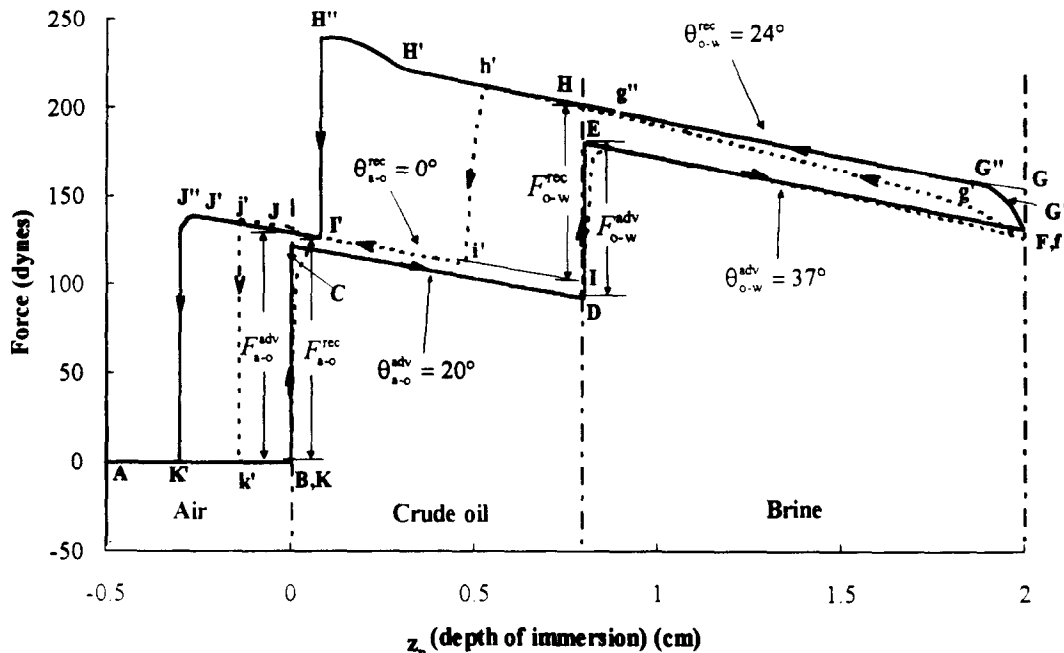


Fig. 9. Experimental and theoretical force versus distance diagrams. Plate (with thin deposit of salt) initially in air.

Calculation of the theoretical curves requires advancing and receding contact angles as part of the input data. These are derived from the force jumps  $F_{a-o}^{adv}$ ,  $F_{a-o}^{rec}$ ,  $F_{o-w}^{adv}$  and  $F_{o-w}^{rec}$  obtained from the experimental data. Backward extrapolation of the linear parts of the diagrams to  $z_p = 0$  (position of the a-o interface) is used to define values of  $F_{a-o}^{adv}$  and  $F_{a-o}^{rec}$  and extrapolation to  $z_p = h$  (position of the o-w interface) defines  $F_{o-w}^{adv}$  and  $F_{o-w}^{rec}$  (see Fig. 9). Application of the foregoing theory to identification of uniform wettability and determination of contact angles requires that part of the curve be linear and that the slope of the curve be consistent with change in buoyancy force. It will be seen that it is sometimes difficult to apply the extrapolation procedure with confidence because experimental data with regions of uniform wetting, as evidenced by slopes that are consistent with change in buoyancy force, are not always obtained.

### 3.1. Plate initially in air

#### Water-wet plate

Force-distance records were investigated for crude oil and brine, using plates which had not been previously contacted with crude oil. The plate was first cleaned and equilibrated in brine. In initial tests, the

plate was removed from the brine, rinsed with distilled water, and dried. When the plate passed from the crude oil into the brine, the water advancing contact angle was close to 90° and the oil-water interface remained essentially flat. When the plate was withdrawn from the water, a low receding angle was observed. However, if the plate was removed from the brine after the equilibration period and simply allowed to dry, the plate gave water-wet behavior for both water advancing and receding conditions as shown in Fig. 9. This example of water-wet behavior was obtained because evaporation of water left a thin deposit of salt, which protected the plate from adsorption while it was lowered through the crude oil. The match between calculated and experimental curves shown in Fig. 9 is generally good, but there are obvious deviations.

The predicted and experimental results are in reasonable agreement for the path ABCDEF. At point F, where the motion changes direction, the interface pins until a lower receding contact angle is established. The distance over which the pinning occurs,  $\overline{fg'g''h'}$ , is much greater than calculated (projection of  $\overline{FG''}$  on the  $z_p$  axis). The likely explanation is that there was slippage of the oil-brine contact line as the plate was raised. Such behavior, which will be described as anomalous pinning, is usually caused by slippage of the three-

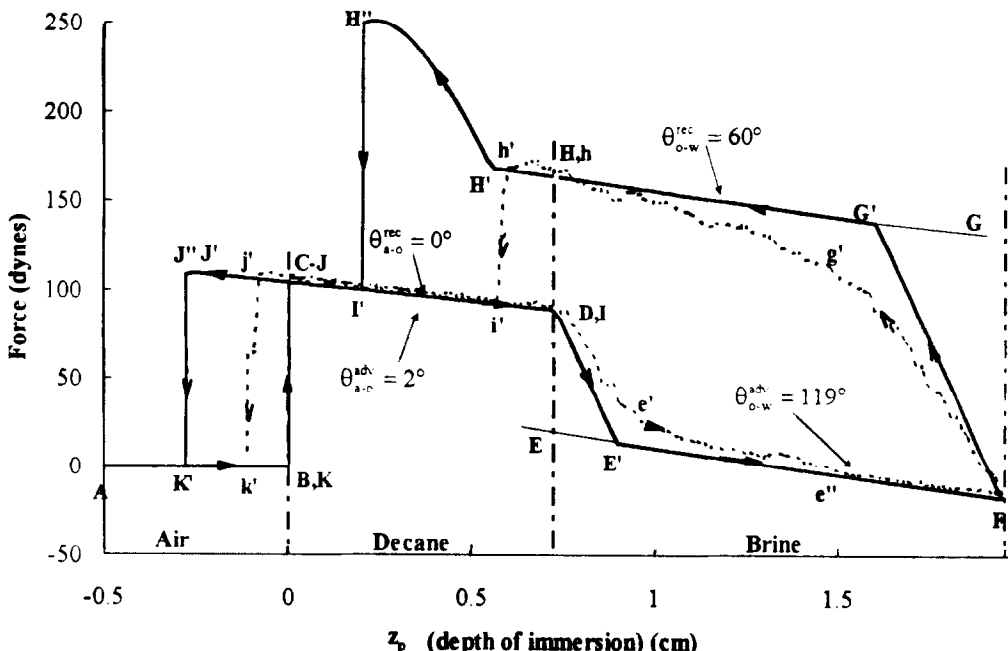


Fig. 10. Experimental and theoretical force versus distance diagrams. Plate initially in air (hybrid wet plate, tested with brine and practical grade decane).

phase line of contact (STPL). STPL is a very common feature of the experimental results. Anomalous pinning can also be caused by trailing films of the displaced phase. In some cases the measured anomalous pinning distance was so long that the buoyancy slope was not established and a stable contact angle could not be identified. Direct observation of interface behavior during the course of the experiment can often aid in identifying the specific cause of anomalous pinning.

Theoretically, the plate can be raised a significant distance above the interface level before the point of detachment illustrated in Figs. 4–6. In practice, slight tilting of the plate, small vibrations, or heterogeneities in wetting, can cause the meniscus to peel away starting from one side of the plate. It can be seen in Fig. 9 that premature detachment corresponding to the jump  $\overline{h'h''}$  occurs well before the predicted jump  $\overline{H''T'}$ . Similarly for the air–oil interface, detachment ( $\overline{j'k'}$ ) occurs well before the jump  $\overline{J''K'}$  predicted by theory. Premature plate detachment is of little consequence with respect to determining adhesion tensions from the force–distance records. However, if the theoretical values could be achieved by experiment, there would be the distinct advantage of obtaining interfacial and surface tensions directly from the force–distance record.

#### Hybrid-wet plate

Fig. 10 shows the force–distance record for a plate that had been treated with crude oil and then (see Table 2 for details of preparation) tested with brine and decane (practical grade). Under these conditions the plate showed hybrid wetting behavior.

During the water advancing stage  $\overline{D'e''F}$ , the anomalous pinning occurs over a longer distance  $\overline{D'e''}$  than the pinning line  $\overline{DE'}$  given by theory. Agreement in the slope of  $\overline{e''F}$  with the theoretical slope shows that a stable contact angle developed over  $\overline{e''F}$ .

When the plate motion is reversed, the predicted curve runs lower than the calculated curve (cf.  $\overline{Fg'h}$  versus  $\overline{FG'H}$  in Fig. 10). A serious problem arises in predicting the water receding contact angle used as input for the calculated results. The experimental portion  $\overline{hh'}$  was used to determine the receding contact angle ( $60^\circ$ ) which was then used to predict the position of the theoretical line  $\overline{G'HH'}$ . The slope of the curve over  $\overline{Fg'h}$  is generally greater than that calculated for buoyancy alone (slope of line  $\overline{GG'H}$ ). Use of a longer plate and a stage that permits a longer traverse would obviously be helpful in checking that the line  $\overline{hh'}$  corresponded to stable wetting.

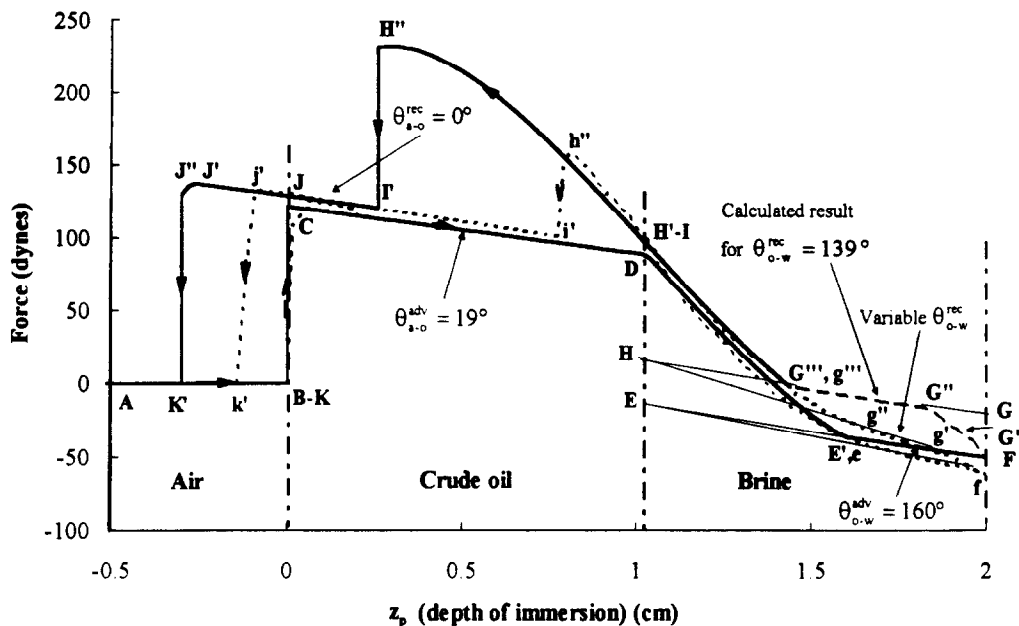


Fig. 11. Experimental and theoretical force versus distance diagrams. Plate initially in air (oil wet plate, tested with brine and crude oil).

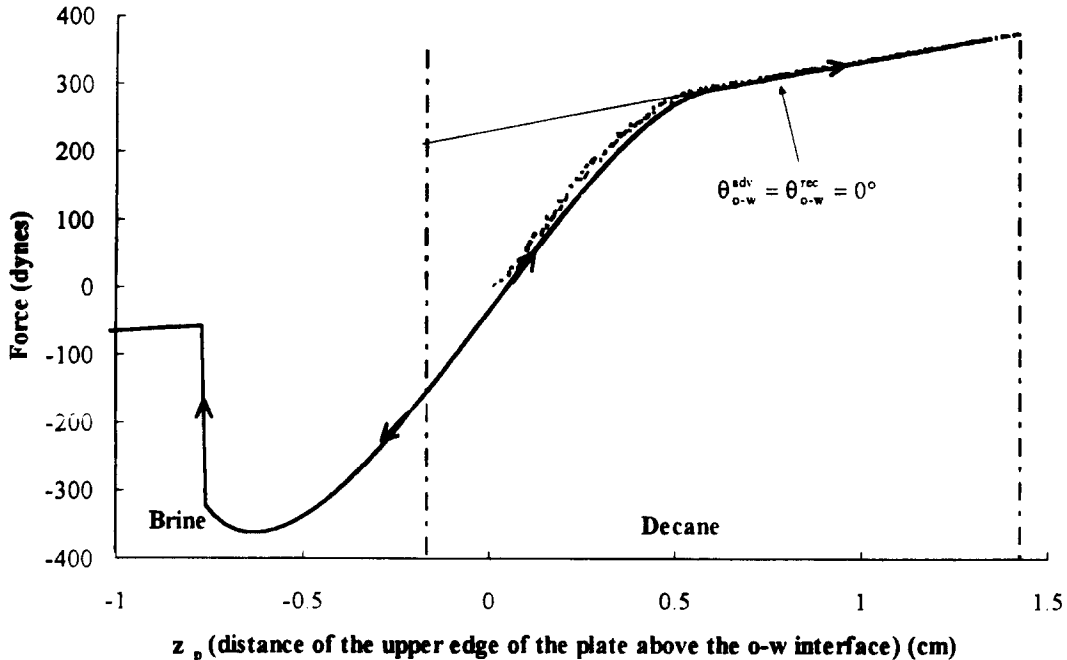


Fig. 12. Experimental and theoretical force versus distance diagrams. Plate initially in brine (water wet plate, tested with brine and decane).

#### *Oil-wet plate*

When the plate was prepared by treatment with crude oil but then tested with crude oil and brine, the force-

distance record showed strong oil wetting for both advancing and receding conditions.

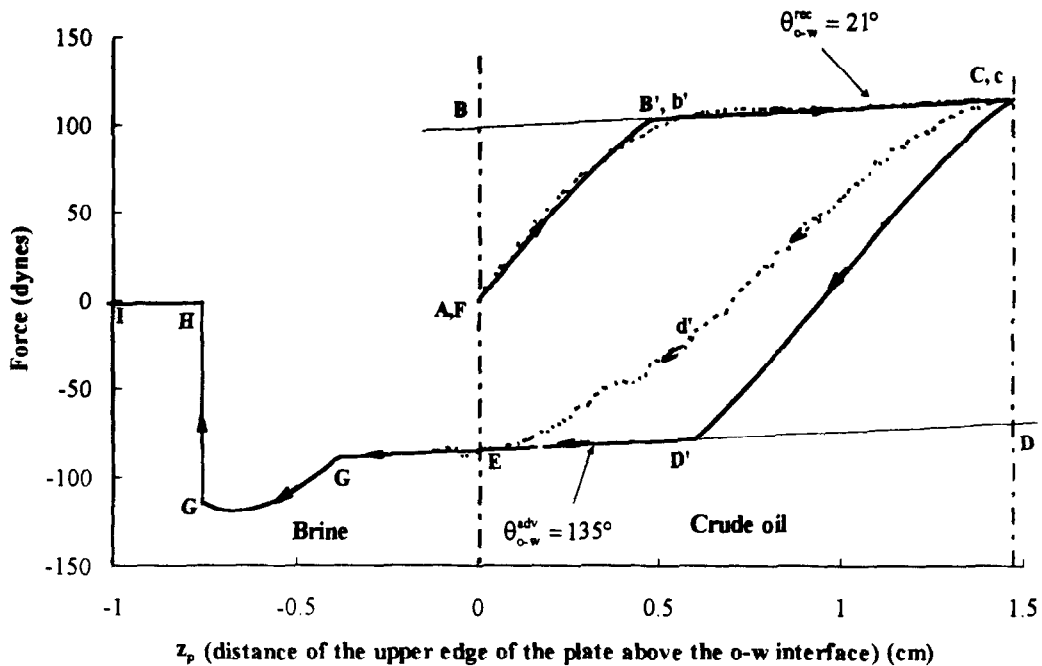


Fig. 13. Experimental and theoretical force versus distance diagrams for hybrid wetting. Plate initially in brine.

Fig. 11 shows the calculated and measured force versus distance curves. For water advancing conditions, the agreement between predicted and experimental results ( $\overline{E'}\overline{F}$  versus  $\overline{e'}\overline{f}$ ) is only fair. The situation is much worse for water receding conditions. There is a reasonably linear portion of the experimental curve,  $\overline{g'}\overline{g}''$ , but the slope is not equal to that of  $\overline{E'}\overline{F}$  which is determined by change in buoyancy. This means that the contact angle is not constant. If the line  $\overline{g'}\overline{g}''$  is used to predict a receding contact angle by extrapolation to H, the predicted result  $\overline{F}\overline{G'}\overline{G}''\overline{G}'''$  (shown as a dashed line) is obtained, which is obviously an invalid match.

A necessary condition of the construction is that  $\overline{g'}\overline{g}''$  and  $\overline{G''}\overline{G}'''$  meet at H. Ideally the two lines should overlap. The smaller the angle between the two lines, the better the fit between experiment and theory. The fit for water advancing conditions ( $\overline{E'}\overline{F}$  versus  $\overline{e'}\overline{f}$ ) is clearly better than that for receding conditions ( $\overline{g'}\overline{g}''$  versus  $\overline{G''}\overline{G}'''$ ).

### 3.2. Plate initially in brine

#### Water-wet plate

Fig. 12 shows calculated and measured force diagrams for a clean water-wet plate tested with brine and decane that had been cleaned by flow through packed columns of silica and alumina. The visual appearance of a water film on the plate confirmed that the plate was perfectly wetted by water. These results demonstrate that very close agreement between theory and experiment is possible for systems that do not exhibit slippage of the three-phase line of contact.

#### Hybrid-wet plate

Fig. 13 shows calculated and experimental force diagrams for a hybrid wet plate. The plate was prepared as outlined in Table 2. The plate was then immersed in brine and a crude oil layer was poured over the brine.

Agreement between experimental and calculated curves was good along the receding path ( $\overline{A}\overline{b'}\overline{c}$ ) but is poor along the advancing path  $\overline{c}\overline{d'}\overline{E}$ . The results for water advancing conditions are dominated by STPL. There is a striking similarity between Fig. 10 and Fig.

13. In one case, a stable contact angle is reached during the advancing path (Fig. 10, path  $\overline{e''f}$ ) and in the other, it is reached during the receding path (Fig. 13, path  $\overline{b'c}$ ). These are the paths of first contact for both tests.

#### 4. Conclusions

(1) In application of the dynamic Wilhelmy plate technique to measurement of adhesion tensions, uniform wetting at the moving three-phase line of contact is indicated by a linear region of the force–distance curve with a slope that matches the predicted change in buoyancy force. These linear regions can be extrapolated to determine the effective advancing and receding contact angles. Experimentally determined contact angles can be incorporated into calculated force–distance diagrams that include contact angle hysteresis, pinning at the three-phase line of contact, and attachment and detachment of the plate from the interface.

(2) Comparison of calculated results with the complete experimental results showed that contact angle transitions from advancing to receding conditions often occurred over much longer distances of plate movement than required by simple pinning. This anomalous pinning is usually caused by slippage of the oil/brine/solid three-phase line of contact.

#### Acknowledgements

The authors are pleased to acknowledge discussions with Jill Buckley and Henry Princen. ENIRICERCHE S.p.A. provided support for Aniello Mennella as a visiting scientist.

#### References

- Adamson, A.W., 1990. *Physical Chemistry of Surfaces*. 5th ed. Wiley, New York, N.Y., pp. 389–411.
- Andersen, M.A., Thomas, D.C. and Teeters D.C., 1989. A new device for determining wetting preference of crude oil/brine/solid systems. *The Log Analyst*, (Sept.–Oct.): 372–381.
- Budziak, C.J. and Neumann, A.W., 1990. Automation of the capillary rise technique for measuring contact angles. *Colloids Surfaces*, 43: 279–293.
- Cuiec, L.E., 1991. Evaluation of reservoir wettability and its effect on oil recovery. In: N.R. Morrow (Editor), *Interfacial Phenomena in Petroleum Recovery*. Marcel Dekker, New York, N.Y., pp. 319–375.
- Fleureau, J.M., 1992. Wettability of reservoir core samples. *SPEFE*, 7(June): 132–138.
- Mennella, A. and Morrow, N.R., 1995. Point-by-point method of determining contact angles from dynamic Wilhelmy plate data for oil/brine/solid systems. *J. Colloid Interface Sci.*, 172: 48–55.
- Princen, H.M., 1970. Advantages and limitations of the Grooved Wilhelmy Plate. *Aust. J. Chem.*, 23: 1789–1799.
- Wilhelmy, L., 1863. Ueber die Abhangigkeit der Capillaritats-Constanten des Alkohols von Substanz und Gestalt des benetzten festen Körpers. *Ann. Physik.*, 119(6): 177–217.